Infrared Spectrum of Poly(l-lactide): Application to Crystallinity Studies

ARTICLE *in* MACROMOLECULES · DECEMBER 2006

Impact Factor: 5.8 · DOI: 10.1021/ma061890r

3 AUTHORS:

Emilio Meaurio
Universidad del País Vasco / Euskal Herriko U…
48 PUBLICATIONS **1,014** CITATIONS
SEE PROFILE

N. López-Rodríguez
Universidad del País Vasco / Euskal Herriko U…
9 PUBLICATIONS **373** CITATIONS
SEE PROFILE

Jose-Ramon Sarasua
Universidad del País Vasco / Euskal Herriko U…
116 PUBLICATIONS **1,703** CITATIONS
SEE PROFILE

Infrared Spectrum of Poly(L-lactide): Application to Crystallinity Studies

E. Meaurio, N. López-Rodríguez, and J. R. Sarasua*

The School of Engineering, The University of Basque Country (EHU-UPV), Alameda de Urquijo s/n. 48013 Bilbao, Spain

Received August 16, 2006; Revised Manuscript Received September 20, 2006

ABSTRACT: The spectrum of PLLA is analyzed in order to investigate its crystallinity and crystalline morphologies. The carbonyl and ester bands of PLLA have been analyzed, and individual components have been successfully assigned. Nucleation always proceeds through curved lamellar crystals, this crystalline morphology being exclusive for low crystallization temperatures. At higher crystallization temperatures, a transition from curved crystals to flat lozenge-shaped lamellae is observed. Curved crystals with edge-on orientation and flat crystals with flat-on orientation affect the intensity of spectral bands. The total crystallinity has been obtained from a skeletal band at 955 cm^{-1}. In addition, intensity changes observed in the C═O stretching region during crystallization provide a simple procedure to obtain the relative population of the two crystalline morphologies. As crystallization temperature increases, the relative population of curved edge-on crystals is observed to decrease, but their population remains important even at the higher crystallization temperatures. The C═O stretching region shows a complex profile that can be fully explained assuming intramolecular through bond coupling and factor group splitting. The latter is also affected by crystalline perfection; hence, the observed crystalline components strongly depend on the crystallization temperature. In the C═O stretching region, perfectly flat crystals give two narrow components at 1767 and 1758 cm^{-1}. Curved crystals obtained at low crystallization temperatures give a broader band located at 1760 cm^{-1} attributed to factor group splitting averaged over the different curvatures shown by this crystalline morphology. This contribution is expected to depend on crystallization temperature according to theoretical considerations (larger nuclei sizes). DSC melting shows a shoulder at lower temperature attributed to the presence of the less stable edge-on crystalline morphology. Finally, the ester C−O stretching region also shows factor group splitting in both the perpendicular (split ∼ 10 cm^{-1}**)** and parallel (split ∼ 18 cm^{-1}) components.

Introduction

Polylactides (PLA) are environment friendly attractive materials that have focused much research effort in recent years.[1] The success of these materials can be attributed to their interesting properties: biodegradable nature, synthesis from renewable sources, thermoplastic manufacturing, and good mechanical properties. Polylactides have found applications in the medical industry to produce biocompatible implant materials that can be eliminated through metabolic mechanisms.[2,3] They also have found industrial applications in the production of plastic parts, films, and fibers.[4,5]

The study of these materials has become a very active field. Most of the studies on solid-state PLA deal with its crystalline structure, but many other aspects regarding solid-state PLA remain unexplored. For example, Kister et al.[6] performed general assignments for the bands observed in the IR spectrum of polylactides. They reported splitting in several bands (including the C═O stretching band), attributed to some conformational sensitivity of unknown origin. The spectral features of PLA have been later discussed in recent papers, but there is no agreement between the different explanations given by different authors.[7−10]

We have recently published a paper in which the C═O stretching region of poly(L-lactide) is explained following a different hypothesis based on the occurrence of splitting in the carbonyl spectral region of low molecular weight compounds of similar chemical structure to that of PLLA.[11] Specifically, diacyl peroxides show two bands in the C═O stretching region, spaced about 25 cm^{-1}.[12] Because their frequencies and relative intensities do not depend on concentration, interassociation and intermolecular interactions can be discarded.[12] Therefore, splitting in diacyl peroxides is attributed to intramolecular coupling of the C═O stretching motions, giving two coupled modes known as symmetric and asymmetric stretching. Because the molecular structure between C═O groups of diacyl peroxides is similar to that of PLLA, intramolecular coupling should be also expected for the latter.

Nevertheless, a higher coupling interaction can be expected in diacyl peroxides compared to PLLA because the former contain two oxygen atoms between adjacent C═O groups.[13] Hence, it seems necessary to look for additional model compounds matching the chemical structure of the main chain of PLLA. The best low molecular weight model compound should be L-lactide, the cyclic dimer of PLLA, but a visual inspection of the IR spectrum of L-lactide does not readily reveal splitting in the C═O stretching region.[14] However, a careful study based on ab initio calculations and virtual circular dichroism (VCD) spectra revealed two bands located at 1786 and 1771 cm^{-1} according to Tam et al.[14] They also noted that splitting is difficult to observe because the symmetric stretching band (higher wavenumbers) shows small relative intensity (nearly 20 times lower) due to C═O groups being only somewhat deviated from a collinear geometry. The splitting of 15 cm^{-1} reported by Tam et al. allows us to apply Miyazawas first-order perturbation theory[15,16] to L-lactide, leading to a perturbation parameter $D_1 = 15$ cm^{-1}. This result is in very good agreement with the value reported by us for PLLA (13.9 cm^{-1}),[11] supporting the same origin for the splitting observed in both systems. In addition, we would want to mention another

* Corresponding author. E-mail: jr.sarasua@ehu.es.

10.1021/ma061890r CCC: $33.50
Published on Web 12/07/2006

model compound for which splitting is easily observed: butyl butyryllactate (CAS # 7492-70-8). The IR spectrum of this compound (Aldrich library) shows clearly two components as in diacyl peroxides,[12] but because of the weaker interaction, the symmetric stretching band is less resolved and appears as a shoulder. Hence, splitting of the C═O band for L-lactide and butyl butyryllactate confirms that a coupling interaction similar to that of diacyl peroxides also occurs in compounds with the skeletal structure of PLLA (−CO−C−O−CO−).

Coupling interactions have been studied mainly in polypeptides, leading to the identification of three coupling pathways: through valence bond, through hydrogen bond, and through space coupling[17−20] (the latter arising from electrostatic dipole−dipole interactions, also known as transition dipole coupling), but there has been some disagreement as to the relative importance of each pathway.[18] In recent works, the problem has been revised in polypeptides labeled to achieve increased resolutions.[17−20] It has been found that through valence bond interactions between adjacent amide groups are essential to explain spectral results, while transition dipole coupling (TDC) interactions are necessary to account for the observed coupling interactions between ^{13}C labels at larger separations. These pathways were also considered in our paper dealing with the carbonyl band of polylactides. These polymers do not show hydrogen bonding;[21] hence, through hydrogen bond coupling can be discarded. Regarding TDC interactions, the independent nature of the spectral shape of diacyl peroxides with concentration[12] clearly proves that intermolecular TDC interactions are not the responsible for the splitting in these compounds (probably they could account for secondary spectral changes, such as slight shifting or bandwidth changes). Hence, it seems also straightforward to neglect intramolecular TDC interactions in diacyl peroxides, just because the distance between carbonyl groups of different molecules is of the same order of magnitude than the distance between carbonyl groups within the same molecule. Also, recent studies on the noncoincidence effect (NCE) of dicarbonyl compounds have reported low NCE values (about 1 cm^{-1}), supporting the weak nature of intramolecular TDC interactions in these compounds.[22] In conclusion, the main splitting observed in PLLA cannot be attributed to TDC interactions, but we agree that these could be present as a second-order effect, shifting slightly the split bands or modifying their width. Hence, it is concluded that the main coupling pathway responsible for the observed splitting in the carbonyl stretching region of diacyl peroxides or polylactides is through valence bond coupling.

In our previous paper,[11] we obtained an equation based on the simple coupled oscillator (SCO) model, useful for the simulation of the IR spectrum of through valence bond coupled vibrational modes of helical polymers. The formalism is similar to that of Snyder et al.,[23−26] who studied mechanical coupling in polymeric chains. It is based in the analysis of a mechanically coupled system (known as the simple coupled oscillator) by means of Newton's laws of motion. The fundamental assumption of this model is harmonic motion for the coupled oscillator set, so that the coupling interaction can be modeled with springs connecting directly the interacting groups. As infrared vibrations are considered harmonic in the first-order approximation, the model can be extended to any harmonically coupled system even if mechanical coupling is not the molecular coupling mechanism.

The SCO model was applied to the carbonyl stretching mode of amorphous PLLA.[11] The conformational energy map of PLLA shows four minima, and only four distinct conformers termed tt, tg, gt, and gg are stable. These conformers form 2_1 (tt), 5_1 (tg), 10_3 (gt), and 4_1 (gg) helixes, respectively, that were built using a software package.[11] It was found that for tt, tg, and gt conformers carbonyl groups are nearly perpendicular to the helical chain. Hence, the total transition moment corresponding to these conformers is perpendicular to the helical chain and shows a nonzero value only for the coupled vibrational modes with a phase angle

$$\phi = \frac{2\pi a}{H} \tag{1}$$

(where ϕ is the phase angle and H is the number of repetitive units contained in a turns). In the case of gg conformers, the individual transition moments orient nearly parallel to the helical chain; hence, only the coupled vibrational mode with $\phi = 0°$ is observed. An important result is that each PLLA conformer shows a single band in the C═O stretching region, instead of the two possible contributions, enormously simplifying this spectral region. It was possible to obtain the conformer population of amorphous PLLA at different temperatures. However, we did not deal with the quantitative analysis of the carbonyl stretching region of crystalline PLLA because additional complicating factors were suspected. In this paper the analysis of the IR spectrum of PLLA is extended to crystalline samples. The carbonyl and ester stretching regions are discussed, and changes observed in the IR spectra are explained considering intramolecular coupling, factor group splitting, and crystal orientation. These three factors can explain all the spectral features observed in crystalline PLLA. In addition, the crystallinity of the samples is obtained from the IR spectra.

Experimental Part

A. Starting Materials. Optically pure poly(L-lactide) containing less than 0.01% of residual solvent and less than 0.1% residual monomer was supplied by PURAC BIOCHEM (The Netherlands). Its specific rotation in chloroform at 20 °C was −157.3°. The molecular weight of poly(L-lactide) was measured viscometrically in a Ubbelohde-type viscometer in chloroform at 30 °C, using the relation[27]

$$[\eta] = 5.45 \times 10^{-4} M_v^{0.73} \quad \text{(dL/g)} \tag{2}$$

A value $M_v = 3.2 \times 10^5$ g/mol was obtained.

B. Infrared Spectroscopy. Infrared spectra of PLLA films were recorded on a Nicolet AVATAR 370 Fourier transform infrared spectrophotometer (FTIR) purged with dry air. Typical samples were prepared by pouring two drops of a 0.8 wt % PLLA solution on $CHCl_3$ over KBr pellets with a Pasteur pipet. The solution is immediately spread over the KBr pellet and allowed to evaporate at room temperature followed by vacuum drying at 50 °C for 48 h, resulting in an absorbance of 0.5 ± 0.2 units. Isothermal crystallizations were recorded in a temperature cell accessory controlled within an accuracy of ±1 °C. Cold crystallizations were carried out in the temperature range 80−100 °C. Samples were heated at 20 °C/min to the desired temperature and isothermally crystallized for an hour. Spectra were collected after 1 min intervals by coadding eight scans at a 2 cm^{-1} resolution, and samples were then allowed to cool to room temperature to obtain room temperature spectra. Melt crystallization was studied in the temperature range 140−165 °C. Samples were heated at 20 °C/min to 200 °C, allowed to melt (complete melting was monitored by inspection of the IR spectrum of the ester CO−O stretching band), and held for 1 min prior to cooling at 5 °C/min to the desired temperatures. Since PLLA is prone to thermal degradation, this step was carefully repeated.[28] IR spectra were collected after 10 min intervals by coadding eight scans at a 2 cm^{-1} resolution during the isothermal crystallizations for 15 h. Second derivatives of the spectra were smoothed with quartic 9- and 13-point Savitzky−Golay smoothing

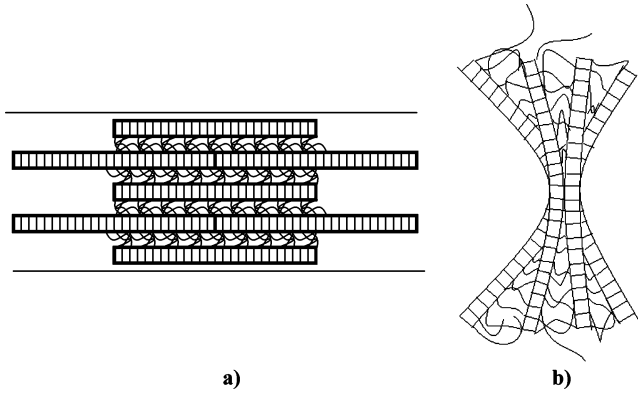

Figure 1. Schematic structures for limiting structures expected in PLLA thin films. (a) Cross view of PLLA film containing flat-on lamellae stacks and (b) top view of PLLA film containing edge-on lamellae.

filters[29,30] in the case of the C=O and ester C−O stretching regions, respectively. Care was taken on the degree of distortion introduced by the smoothing algorithm, checked according to the procedure reported elsewhere.[31]

C. Film Thickness Measurement. 50 drops of the 0.8 wt % PLLA solution were evaporated over a Petri dish and dried under vacuum. The mean weight of polymer contained in two drops of the polymer solution was 0.13 mg. Considering the diameter of the KBr pellets (13 mm), the molar volume of the repetitive unit of PLLA (53.3 cm^3/mol),[31] and its molecular weight (72 g/mol), a mean thickness of 0.72 μm is obtained.

D. DSC Analysis. Thermal analysis was carried out on a DSC from TA Instruments, model DSC 2920. Approximately 5−10 mg of polymer was weighted and sealed in an aluminum pan. Samples were crystallized following similar heating ramps to that used in FTIR measurements. For cold crystallization studies, they were heated at 20 °C/min to the desired temperatures and maintained for an hour. Sample crystallinity was obtained in the consecutive scan at 20 °C/min, after slow cooling to room temperature. In melt crystallization studies, they were first heated to 200 °C at 20 °C/min, maintained for 1 min, and then cooled to the desired temperatures at 5 °C/min and allowed to crystallize for 15 h. Finally, it was slowly cooled at 2 °C/min to room temperature, and crystallinity was obtained from the DSC curve recorded in the subsequent scan at a heating rate of 20 °C/min.

Results and Discussion

Considering the thickness of the FTIR films studied in this work (below 1 μm, see Experimental Part), crystalline morphologies similar to those observed in thin films are expected.[32−34] Atomic force microscopy (AFM) studies on thin films of PLLA crystallized from the melt show that S-shaped edge-on lamellae are formed during nucleation and the initial stages of crystallization.[34] As the crystals grow, a transition from edge-on to flat-on crystals is observed; afterward, crystallization proceeds only through flat-on crystals. A negligible influence of film thickness on the lamellar orientation is found, and the orientation is derived from the air−polymer interface rather than the effect of substrate.[34] In the case of the cold crystallized samples studied in this work, the same nucleation morphology can be expected, but because cold crystallizations proceed very fast, we do not expect a transition from edge-on to flat-on crystals. Experimental evidence of this assumption is found by observing the similitude of Figure 4a from ref 9 (obtained from a sample cold crystallized at 80 °C) and Figure 1c from ref 36. The "fibrillar crystallites" obtained in the former closely resemble edge-on lamellar crystals. Regarding the structure of melt crystallized films, flat on lamellar crystals can be expected to be dominant in films crystallized at the higher temperatures. These crystals form lozenge-shaped lamellae that grow until mutual impingement.[34] As their thickness is about 10 nm, several layers can be expected in the ∼700 nm thick films studied in this work. The limit structures for both cold and melt crystallized samples are shown in Figure 1. Finally, the formation of molecular order in the amorphous regions between the lamellar stacks of Figure 1a has been well documented for polymers with stiff chains.[35−37] In our previous paper on the FTIR spectrum of PLLA, we observed narrow bands for noncrystalline components, which were attributed to such semiordered structures.[11]

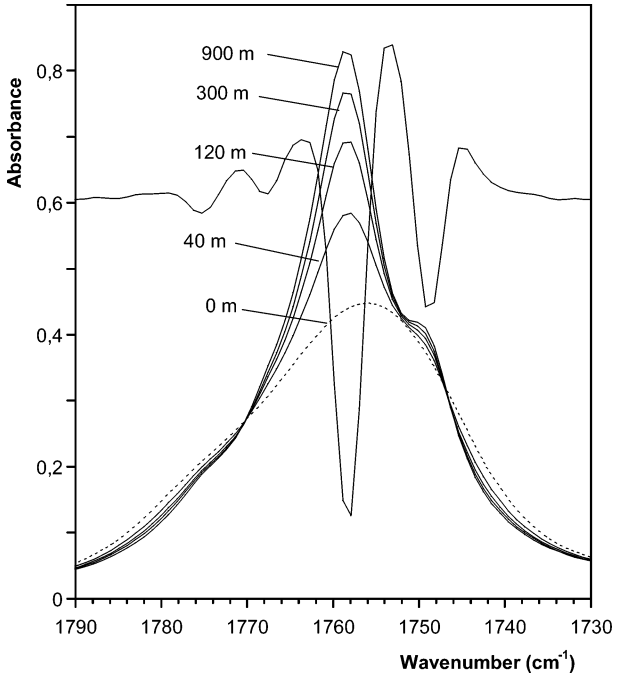

Figure 2. Carbonyl stretching region of PLLA and second derivatives recorded during isothermal crystallization at 90 °C. The spectra of amorphous PLLA are highlighted with a dotted line.

A. The C=O Stretching Region. Figure 2 shows the spectrum of PLLA crystallized from the melt at 160 °C for 15 h. These crystallization conditions are spectroscopycally favorable over those of ref 11 because they lead to enhanced spectral changes during crystallization (arising mainly from longer crystallization times and a favorable crystal orientation). The second-derivative spectrum shows four components at about 1749, 1758, 1767, and 1776 cm^{-1}, which were assigned to tt, gt, tg, and gg conformers, respectively. These assignments are strongly supported from a experimental point of view because (i) they fit the dispersion curve corresponding to intramolecular coupling, giving an interaction parameter similar to that obtained for L-lactide (D_1 = 13.9 cm^{-1} in PLLA vs D_1 = 15 cm^{-1} in L-lactide; see introduction); (ii) components assigned to tt, gt, and gg conformers were also observed in the spectrum of amorphous PLLA,[11] showing similar contributions to those of Figure 2; and (iii) they are also observed in the ATR spectra of amorphous samples. But in light of Figure 2, we find difficult to assign the contribution observed at 1767 cm^{-1} only to tg conformers. The main objection is the increase of absorption observed during crystallization, suggesting a crystalline contribution instead of a amorphous one. In addition, the population measured for tg conformers in amorphous PLLA was small (they were not even discerned in the second-derivative spectra),[11] and it seems difficult to assign all the absorption at this location to the most unstable conformers.

The increase of absorption at 1767 cm^{-1} during crystallization can be attributed to factor group splitting (also called correlation

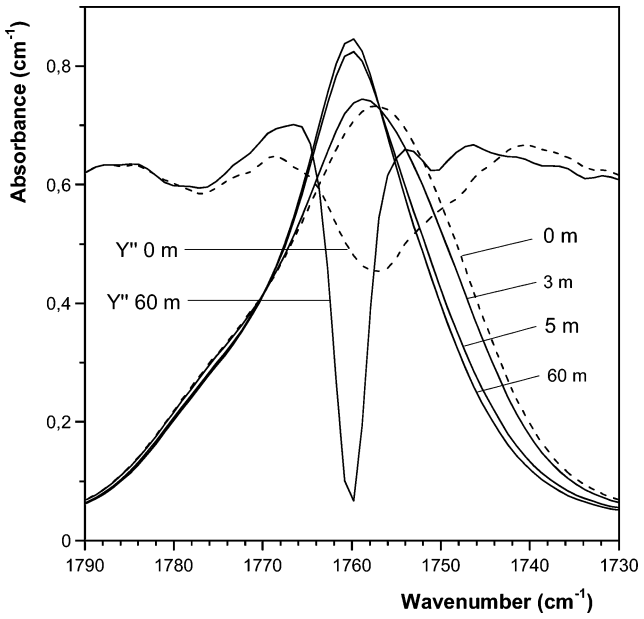

Figure 3. Carbonyl stretching region of PLLA and second derivatives recorded during isothermal crystallization at 90 °C. The spectra of amorphous PLLA are highlighted with a dotted line.

field splitting or Davydov splitting).[38,39] Factor group splitting occurs due to lateral interaction between the chains contained in the unit cell, splitting the absorption in a number of components identical to the number of chains contained in the unit cell. In the case of the orthorhombic unit cell of PLLA, the transition moments of the two adjacent PLLA chains can couple in phase or out of phase, splitting the IR absorption in two bands. According to this simple description of the factor group splitting phenomenon, the new bands should be centered in the location of the unperturbed absorption (similarly to the splitting in a symmetric and an asymmetric stretching band found in dicarbonyl compounds), but this is not actually observed and repulsive potentials have been claimed to explain shifting to higher wavenumbers.[40] The most representative example of factor group splitting is found in the CH_2 rocking mode of polyethylene. The spectrum of amorphous polyethylene shows a broad peak ($\sim$20 cm^{-1}) at about 723 cm^{-1}, which after crystallization splits in two new narrow peaks at 730 and 722 cm^{-1}, associated with factor group splitting.[41] These peaks can be used to obtain the crystallinity of polyethylene samples by means of a curve-fitting procedure because the amorphous and crystalline peaks at 723 and 722 cm^{-1} are highly overlapped.[42] The actual splitting proposed in this paper for PLLA closely resembles that observed for the CH_2 rocking mode in polyethylene. We suggest that the crystalline absorption of the carbonyl stretching band of PLLA splits in two components located at 1758 and 1767 cm^{-1}, the former being highly overlapped with the contribution of gt conformers corresponding to the semi-ordered interphase. We will also show in this paper that a very similar behavior is also observed in the ester (C−O) stretching region.

Figure 3 shows the spectra obtained in the C═O stretching region during the cold crystallization process of PLLA at 90 °C, indicating important structural differences with melt-crystallized samples. A single crystalline peak located at 1760 cm^{-1} is observed instead of the pair of peaks at 1758 and 1767 cm^{-1} that were observed in samples crystallized from the melt. In addition, the second derivative of a completely amorphous sample reveals that the location corresponding to gt conformers is 1758 cm^{-1}. It is known that factor group splitting is highly sensitive to crystalline order,[38,39] and observing the AFM images of edge-on crystals,[34] different curvatures can be observed for the different edge-on crystals. Larger factor group splitting can be expected for the more rectilinear crystals and lower splitting for the more curved ones. Hence, the crystalline band at 1760 cm^{-1} is attributed to factor group splitting averaged over the distribution of different crystal shapes observed for edge-on crystals. Table 1 compiles the spectral components that can be found in the C═O stretching region of the PLLA samples studied in this work.

There is also another interesting result if Figure 3 that needs to be considered. Comparison with Figure 2 reveals that the amorphous conformers of cold crystallized samples do not show narrow peaks, suggesting that they retain their initial disordered arrangement. In addition, the decrease of absorption at 1777 cm^{-1} (gg conformers) is clearly smaller than that observed in the 1740−1760 cm^{-1} range (corresponding to gt and tt conformers), suggesting a preferred consumption for the latter. Probably, this behavior is related to the high viscosity of the sample during crystallization at lower temperatures, where the most crowded conformers find increased difficulties to orient and pack in the lamellae. Hence, another conclusion must be drawn: the amorphous phase can be considered disordered (because of the width of the spectral bands) but not completely random because it does show the same population distribution as the initial amorphous phase (in other words, it does not obey the same Boltzmann statistics).

The progress of crystallization has been followed by the intensity change ratio $(H_t - H_0)/(H_\infty - H_0)$, where H_0, H_t, and H_∞ represent the peak height of the original sample, crystallized for a time t, and after completion of the crystallization, respectively. The intensity change ratio as a function of crystallization time is plotted in Figure 4a, based on data obtained from the band at 1182 cm^{-1} (attributed to C−O stretching). As can be seen, cold crystallization proceeds very fast; in fact, crystallization can be considered almost complete in the initial 5 min for samples crystallized above 90 °C. However, for melt-crystallized samples (Figure 4b) longer crystallization times (from 2 to 5 h depending on temperature) are necessary to complete primary crystallization, and afterward a slowly progressing secondary crystallization can be observed. Nevertheless, according to Figure 4a,b complete primary crystallizations can be assumed for both cold and melt crystallized samples. Finally, we want to note that cold crystallization samples have shown final crystallinity contents much lower that samples crystallized from the melt, but in spite of this, cold crystallized crystals remain imperfect. This peculiar crystallization behavior has been reported in recent papers.[9,52]

Another interesting difference between cold and melt crystallized samples is the intensity change observed in the C═O stretching band during the crystallization process (readily observed by comparing Figures 2 and 3). Areas obtained after the crystallization process are listed in Table 2 and have been plotted in Figure 5. Cold crystallization leads to a decrease of the total area of the C═O stretching band about 9% irrespective of the crystallization temperature. The decrease of area is attributed to the change of orientation from an amorphous sample to a edge-on crystalline sample (see Appendix). On the other hand, crystallization from the melt leads to an increase of area depending on the crystallization temperature. As crystallinity degrees for melt crystallized samples are similar (Table 2), the observed variation should be explained assuming a increased population of flat-on crystals relative to edge-on crystals as temperature increases.

Table 1. Spectral Contributions Observed in Amorphous, Cold Crystallized, and Melt Crystallized PLLA Samples

	wavenumber (cm^{-1})	assignment	comments
noncrystalline components	1777	gg	present in all PLLA samples; the band at 1767 cm^{-1} is weak (higher energy conformers); in samples crystallized from the melt, these bands show narrow profiles, attributed to a semiordered interphase between lamellae stacks
	1767	tg	
	1759[a]	gg	
	1749	tt	
crystalline components	1760	gt (FGS[b] av)	present in all crystalline samples; as crystallization temperature increases, this component may shift/split due to higher crystlline perfection
	1758	gt (split)	only present in samples crystallized from the melt
	1767	gt (split)	

[a] According to the second derivative of amorphous samples, 1758 cm^{-1} should be more appropriate. Because 1 cm^{-1} is a small difference, the accepted mean value is adopted. [b] FGS refers to factor group splitting.

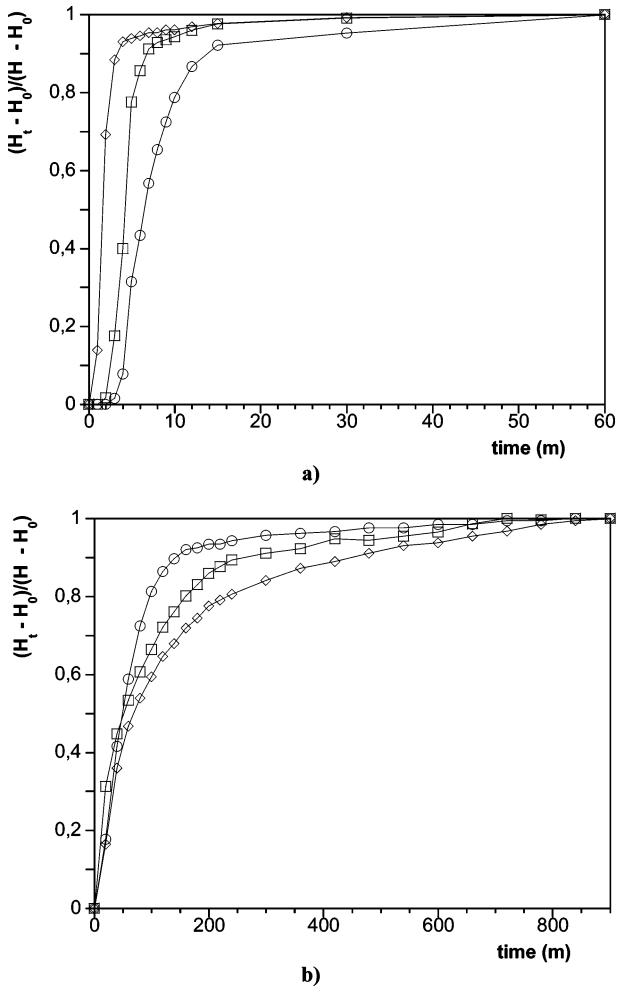

Figure 4. Crystallization progress followed by the intensity change ratio for (a) isothermal cold crystallization at (○) 80, (□) 90, and (◇) 100 °C and (b) isothermal melt crystallization at (○) 140, (□) 150, and (◇) 160 °C.

In addition, the data in Figure 5 allow the determination of the transition temperatures between crystallization regimes. According to the crystallization theory of Lauritzen and Hoffman,[43] the crystallization range of a polymer is divided into three regions or regimes that are dictated by the rates of two processes, namely secondary nucleation and lateral spreading or growth. The rates of these processes are represented as *i* and *g*, respectively. In this paper, cold crystallization has been studied in regime III ($i \gg g$), and the transition to regime II (*i* comparable to *g*) is found to occur at 116 °C, in good agreement with the value reported in the literature (about 115 °C).[44] In addition, the transition to regime I ($g \gg i$) is suggested to occur at about 160 °C (experimental value is 163 °C).[44]

Table 2. Area of the C═O Stretching Band after Isothermal Crystallizations; Crystallinities (X_c) Calculated from the Band at 955 cm^{-1} and Eq 3; Crystallinities Corresponding to Edge-On (X_{ce}) and Flat-On Crystals (X_{cf}) According to Eq 7; and Crystallinities Obtained by DSC for Samples with Similar Thermal Histories

cold crystallized samples

crystallization temp (K)	final area of C═O stretching band[a]	X_c (%) IR	X_c (%) DSC[b]
80	90.9	36	26
90	91.1	35	28
100	90.9	35	25

melt crystallized samples

crystallization temp (K)	final area of C═**O** stretching band[a]	X_c (%) IR	X_{ce} (%) IR	X_{cf} (%) IR	X_c (%) DSC[b]
140	105.9	50	26	24	52
145	108.3	56	26	30	
150	112.1	60	24	36	55
155	115.2	62	21	41	
160	118.0	65	19	46	59
165	117.6	62	18	44	

[a] Measured between 1600 and 1900 cm^{-1}. All the spectra have been normalized setting the area for the initial amorphous spectrum to 100 arbitrary units. [b] Calculated using a melting enthalpy $\Delta H_f = 106$ J/g for 100% crystalline PLLA.[46]

B. Crystallinity of PLLA Films. The simplest way to obtain the crystallinity of PLLA samples relies on the area of an amorphous band at 955 cm^{-1}. During crystallization, the intensity of this band decreases and a new band appears at 921 cm^{-1}, characteristic of α crystals (see Figure 6). According to 2D correlation analysis, the decrease of area of the band at 955 cm^{-1} is synchronized with the increase of area of the band at 921 cm^{-1}.[7] Both bands are well resolved, and a quantitative determination of crystallinity is easy from the percent area loss of the band at 955 cm^{-1}:

$$X_c = \frac{I_0 - I_f}{I_0} \times 100 \qquad (3)$$

From the area of the band at 955 cm^{-1} in the initial amorphous sample (I_0) and the area measured after crystallization (I_f), crystallinity degrees have been obtained for the samples studied in this work (Table 2). The crystallinity of cold crystallized samples is about 35%, slightly higher than the values obtained by DSC. For samples crystallized from the melt, there is a reasonable agreement between results obtained by DSC and FTIR. In this case, as crystallization of PLLA samples strongly depends on melting conditions,[28] DSC and FTIR results should be compared with caution because identical thermal histories cannot be assured.

The crystallinity degree can be also calculated from the changes of area observed for the C═O stretching band.

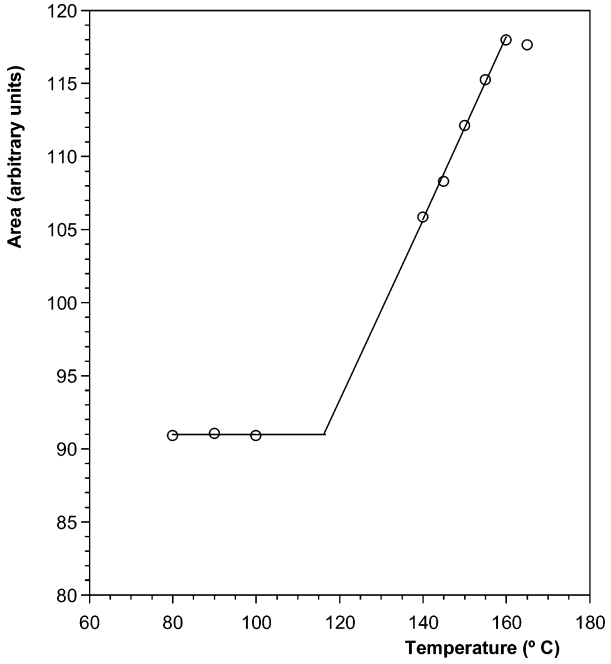

Figure 5. Area of the carbonyl stretching region of PLLA between 1600 and 1900 cm^{-1}, after isothermal crystallization at the indicated temperatures. All areas were measured at room temperature, and 100 arbitrary units were assigned to the initial amorphous spectrum.

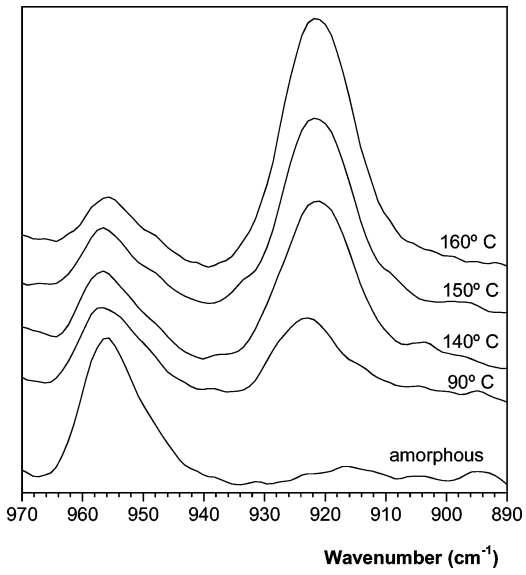

Figure 6. Spectra in the 890−970 cm^{-1} region for samples crystallized at different temperatures, normalized using the initial area of C═O stretching band. Crystallinities have been calculated from the area loss for the band at 955 cm^{-1} according to eq 3.

Considering the coefficients obtained in the Appendix, complete crystallization of an amorphous sample to edge-on crystals should lead to a decrease of area of 25% for the carbonyl stretching band. The experimental area decreases about 9%; hence, crystallinity can be calculated from

$$X_c = \frac{\%\ \text{area decrease}}{25} = \frac{9}{25} \times 100 = 36\% \qquad (4)$$

This result is in good agreement with that obtained from the band at 955 cm^{-1}. There are two relevant assumptions in this calculation: first, all the crystals are considered perfectly vertical; second, $\epsilon_C/\epsilon_A = 1.0$. Assuming similar molar extinction coefficients for the amorphous and crystalline phases is reasonable from a theoretical point of view because the refractive index change accompanying a crystallization process has only a subtle effect on the absorptivity[45] and orientation effects are fully excluded in the preceding absorptivity ratio. Hence, the change of area of the C═O stretching band can be also considered to monitor the crystallinity of PLLA samples.

The crystallinity differences observed by FTIR and DSC for cold crystallized samples are beyond experimental error. In our opinion, DSC values are probably underestimated because they are calculated using a melting enthalpy $\Delta H_m^0 = 106$ J/g,[46] corresponding to a perfect infinite crystal. This value gives good correlation between crystallinity values obtained by WAXS and DSC for highly crystalline PLLA samples ($\chi_c = 70\%$).[52] However, cold crystallized samples consist mainly on imperfect crystals that may show a different thermal behavior compared to that of the perfect crystal. In fact, in a recent paper, Mano et al.[53] have measured by WAXS the crystallinity of cold crystallized PLLA samples, obtaining values around 32−35%, in good agreement with our FTIR results. They also observed that the best agreement with DSC crystallinities was obtained choosing smaller values for the enthalpy of fusion of the perfect crystal. However, only a single value can be attributed to the perfect crystal, and the better correlation obtained with smaller values for ΔH_m^0 suggests additional contributions to the measured melting enthalpies of cold crystallized samples, such as higher interfacial energies.

Areas obtained in the C═O stretching region can be also applied to obtain the crystallinity of samples crystallized from the melt, leading to interesting results. According to AFM studies,[34] both edge-on and flat-on crystals can be expected, the former being located in crystal nuclei. Because the change of area upon crystallization strongly depends on the crystallization temperature (Figure 5), larger amounts of edge-on crystals can be expected for the samples crystallized at lower temperatures. The presence of a significant amount of edge-on crystals even for the samples crystallized at the higher temperatures is supported by the contribution at 1200 cm^{-1} (see next section). Considering the coefficients obtained in the Appendix, complete crystallization of an amorphous sample to flat-on crystals should lead to an increase of area of 50% for the carbonyl stretching band. Hence, for samples crystallized form the melt, the following set of equations can be written:

$$0.5X_{cf} - 0.25X_{ce} = \Delta A \qquad (5)$$

$$X_c = X_{ce} + X_{cf} \qquad (6)$$

where X_{cf} is the crystallinity degree corresponding to flat-on crystals, X_{ce} is the crystallinity degree corresponding to edge-on crystals, and ΔA is the percent area variation of the C═O stretching band. Hence

$$X_{cf} = \frac{X_c + 4(\Delta A)}{3} \qquad (7)$$

Using X_c values obtained from the band at 955 cm^{-1} and the changes of area measured for the C═O stretching band, it is possible to quantify the percentages of edge-on and flat-on crystals. Results are summarized in Table 2. As can be seen, the population of edge-on crystals is comparable to that of flat-on crystals for samples crystallized at 140 °C, but as crystallization temperature increases, the population of edge-on crystals decreases. However, the contribution of edge-on crystals does not become negligible even at the higher crystallization tem-

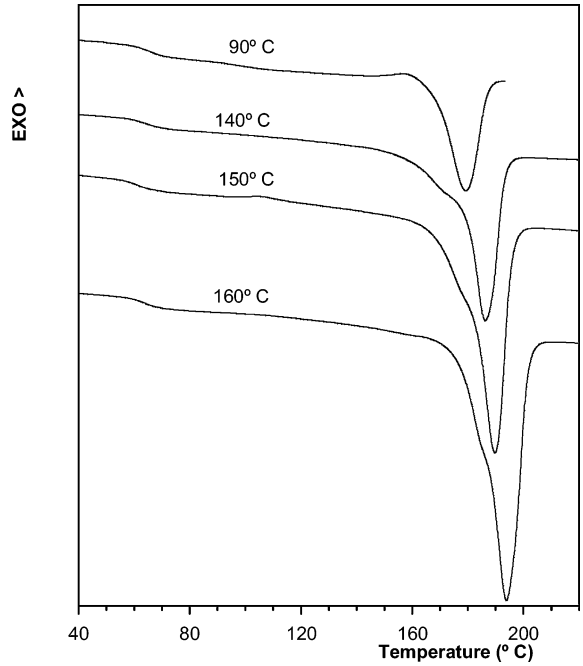

Figure 7. Melting scans for PLLA samples crystallized at the indicated temperatures.

peratures. Values of X_{ce} in Table 2 actually reflect the product (number of nuclei) × (size necessary for transition from edge-on to flat-on) at each crystallization temperature. The mechanism responsible for the transition is at present not fully understood,[34] but it is possible to explain the behavior of X_{ce} values in Table 2 by comparison with the behavior of critical nucleation sizes. The number of nuclei is known to decrease as crystallization temperature increases, but their critical size increases;[33] hence, a lower number of larger nuclei can be expected at higher crystallization temperatures. The same trend should be expected for the population of the edge-on crystals. Hence, FTIR results suggest that although the number of nuclei decreases as temperature increases, their larger transition size leads to a significant contribution for edge-on crystals even at the higher crystallization temperatures.

The coexistence of edge-on and flat-on crystals in melt crystallized samples is also supported by DSC scans. Figure 7 shows DSC curves for samples isothermally crystallized at 90 °C for 1 h and at 140, 150, and 160 °C for 15 h. As can be seen, the sample crystallized at 90 °C shows a melting peak preceded by an exothermal event. This peculiar exothermal event has been attributed to recrystallization of the less thermally stable crystals formed during cold crystallization, which were assigned to a new modification named the α′ form.[9] In addition, PLLA samples crystallized from the melt at 140, 150, and 160 °C show a shoulder. This multiple peak behavior has been observed recently,[47] although the origin for the different peaks could not be established. According to our FTIR results, the lower temperature melting peak can be attributed to the nuclei-forming S-shaped lamellar crystals, while the higher temperature peak is attributed to flat lamellar stacks formed during crystal growth. As can be seen in Figure 7, the melting temperature of both crystals increases with higher crystallization temperature, suggesting higher and more perfect crystals as crystallization temperature increases.

Finally, the existence of weaker crystals in the nuclei of melt crystallized samples has also been observed in previous studies. Fischer et al.[54] studied the hydrolysis of PLLA films, attacking with solutions containing sodium hydroxide. The micrographs obtained showed degradation of the center of the spherulites in significant extent compared to the outer regions.

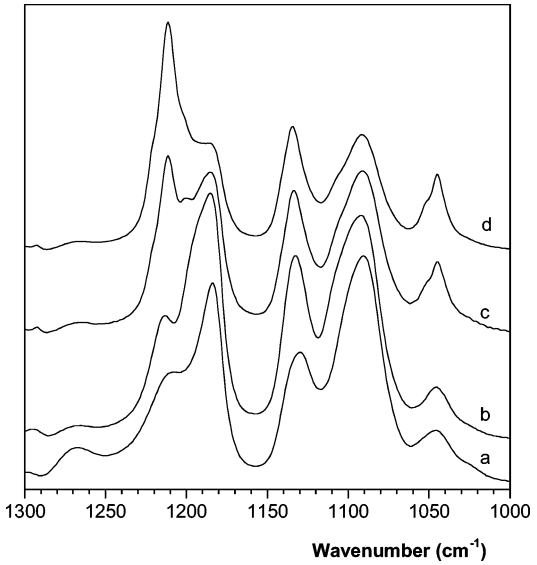

Figure 8. Spectra of PLLA at room temperature after different thermal treatments: (a) amorphous PLLA; (b) cold crystallized at 90 °C for an hour; (c) melt crystallized at 140 °C for 15 h; (d) melt crystallized at 160 °C for 15 h. All the spectra have been normalized using the area of the C═O stretching region of the initial amorphous sample and have been shifted for an easier visualization.

Table 3. Assignments for the Bands Observed in the 1000−1300 cm^{-1} Spectral Region of Amorphous PLLA

IR frequency (cm^{-}1)	assignment
1268	ν(CH) + ν (C−CO−O)
1212	ν_{as}(C−CO−O) + r_{as}(CH_3)
1182	ν_{as}(C−CO−O) + r_{as}(CH_3)
1133	r_s(CH_3)
1089	ν_{as}(O−C−CO)
1044	ν (C−CH_3)

C. The C−O Stretching Region. The "C−O stretching vibrations" of esters consist of two asymmetrical coupled vibrations: C−CO−O and O−C−C, the former being more important.[48] In papers dealing with the IR spectrum of PLLA, they have been referred as asymmetric C−O−C stretching and symmetric C−O−C stretching modes,[6−8] but these vibrational modes are actually characteristic of alkyl ethers. However, in ester compounds the ester CO−O bond is in resonance with the carbonyl group and the two C−O bonds are no longer identical. In this paper, we will follow the abbreviated descriptions found in ref 14, and the ester stretching modes of PLLA will be referred to as the C−O (ester) and C_α−O modes, respectively.

Figure 8 shows the spectrum of amorphous PLLA in the 1000−1300 cm^{-1} region (see Table 3). The C−O stretching region of amorphous PLLA ranges from 1150 to 1300 cm^{-1} and shows three contributions. The interesting bands are located at 1182 and 1212 cm^{-1}, and the band at 1268 cm^{-1} plays only a minor role limited to absorptivity transferences with the two fundamental bands. The band at 1182 cm^{-1} is assigned to an A mode (parallel to the helix) and the band at 1212 cm^{-1} to an E_1 mode (perpendicular to helix axis). We have also explored the possibility of a similar conformational sensitivity to that observed in the C═O stretching region but observed band locations do not fit a dispersion curve assuming intramolecular coupling.[11] The different sensitivity of the C═O and C−O stretching modes can be attributed to their different nature. The carbonyl stretching mode is admitted to be mainly isolated from

Table 4. Assignments for the Spectral Components Found in the Ester C−O Stretching Region of the Samples Studied in This Work; All the Crystalline Samples Show Factor Group Splitting

	IR frequency (cm^{-1})	
	A mode	E_1 mode
amorphous PLLA	1182	1212
PLLA/PDLA 1:1	1199/1182	1221/1212
PLLA melt cryst[a]	1200/1182	1222/1212
PLLA cold cryst[b]	1196/1182	1215

[a] In this system, the lower wavenumber component is overlapped with narrow bands attributed to the semiordered interphase. Also, in samples crystallized in the low-temperature range (below 140 °C), imperfect edge-on crystals may contribute with poorly resolved bands. [b] This system shows broader bands, attributed to averaged factor group splitting over the distribution of curved crystalline morphologies. In the case of the E_1 mode, only a component is resolved.

the polymer chain; hence, C═O groups can be adequately represented by springs directly connecting the carbonyl groups. On the contrary, C−O stretching modes are coupled not only with vicinal CH or CH_3 groups (see Table 4) but also with skeletal modes. This complex coupling pattern results in strongly mixed bands, from which conformational information cannot be obtained.

We will start the analysis of the C−O stretching region using the results obtained in the PLLA/PDLA 1:1 stereocomplex, prepared from the equimolar mixture of the two stereoisomers of polylactide.[21] The PLLA/PDLA stereocomplex crystallizes in a conformation very similar to that of PLLA: the unit cell of the former contains two 3_1 helical chains, while the unit cell of the latter contains two 10_3 helical chains. IR spectroscopy is sensitive to conformation but shows only a very limited sensitivity to long-range order (through reduced bandwidths and factor group splitting); thus, similar spectra can be expected for both samples. It was found that when the stereocomplex crystallizes, the amorphous phase remains completely disordered,[21] resulting in an easier identification of crystalline spectral contributions in this system because narrow peaks corresponding to the amorphous phase are not expected, especially in the second-derivative spectra. Figure 9 shows the spectral changes observed during isothermal crystallization at 200 °C, after cooling from the melt at 250 °C. At 200 °C, the initial amorphous spectrum shows two bands at about 1180 and 1210 cm^{-1}, assigned to the C−O stretching components parallel and perpendicular to the helix axis, respectively. During crystallization, new narrow contributions develop at about 1195 and 1216 cm^{-1}. Since amorphous contributions provide broad bands, the narrow bands observed in the second-derivative spectrum during crystallization should be attributed to crystalline components. Again, as was observed in the C═O stretching region, factor group splitting can explain the presence of four crystalline bands. At room temperature (Figure 10), the two pairs of factor group split bands are located at 1182/1199 and at 1212/1221 cm^{-1}. The increased splitting resolution resulting on cooling is typical of factor group split bands. The parallel band shows a large split of about 17 cm^{-1}, indicating strong contact in this direction. The perpendicular band shows a moderate split of 9 cm^{-1}, similar to that observed in the C═O stretching region, or in the $-CH_2-$ rocking mode of polyethylene.

Figure 11 shows the spectra of a PLLA sample crystallized from the melt at 150 °C. As can be seen, crystallization leads to a decrease of absorptvity at 1268 cm^{-1}, which is transferred to the stretching modes at lower wavenumbers. This is a general trend, also readily observed in the stereocomplex (Figure 8), but in the case of the crystallization of PLLA at 150 °C it

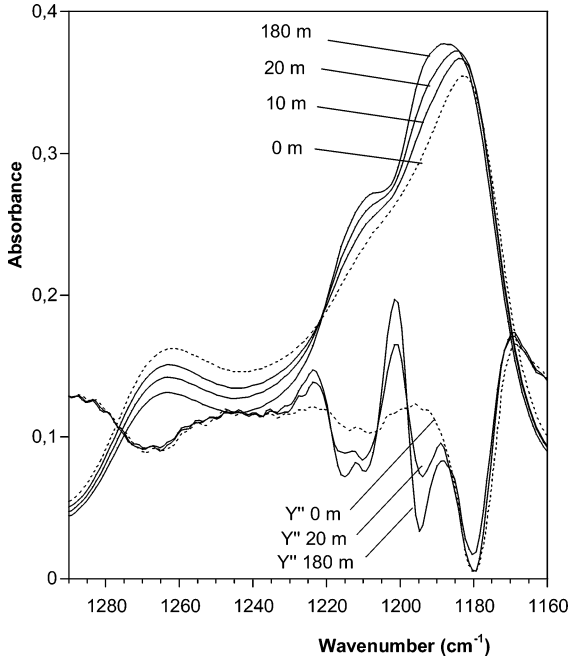

Figure 9. Ester C−O stretching region of PLLA/PDLA 1:1 stereocomplex and second derivatives recorded during isothermal crystallization at 200 °C. The spectrum of completely amorphous blend is highlighted with a dotted line.

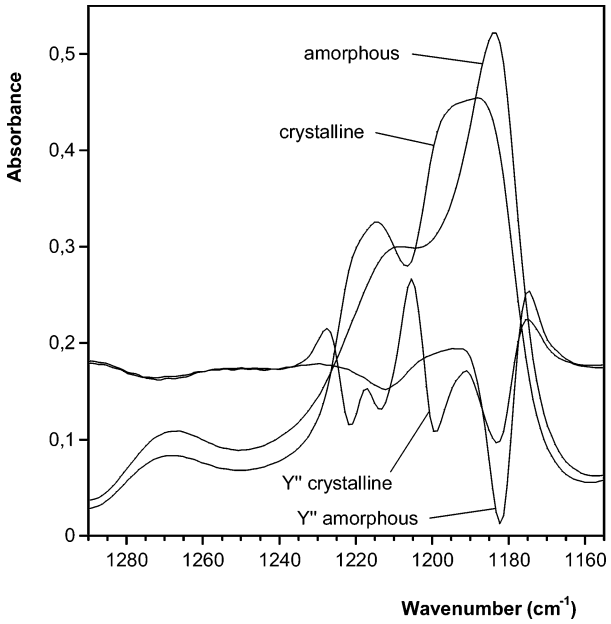

Figure 10. Ester C−O stretching region of PLLA/PDLA 1:1 stereocomplex and second derivatives recorded at room temperature before and after isothermal crystallization at 200 °C for 3 h.

seems to revert mainly in the perpendicular component. This is due to the orientation of the crystals at this crystallization temperature. The perpendicular component increases because in addition to the mentioned absorptivity increase, the transition moments corresponding to gt conformers change their orientation from a random arrangement to a in-plane orientation (formation of flat on crystals). In the case of the parallel band, crystallization leads to a loss of this contribution because it is perpendicular to the plane containing the sample. At 150 °C, this absorption loss is partially compensated by the absorptivity transfer from the band at 1286 cm^{-1}. Because at higher crystallization temperatures the population of flat-on crystals is favored over edge-on crystals, spectra recorded at

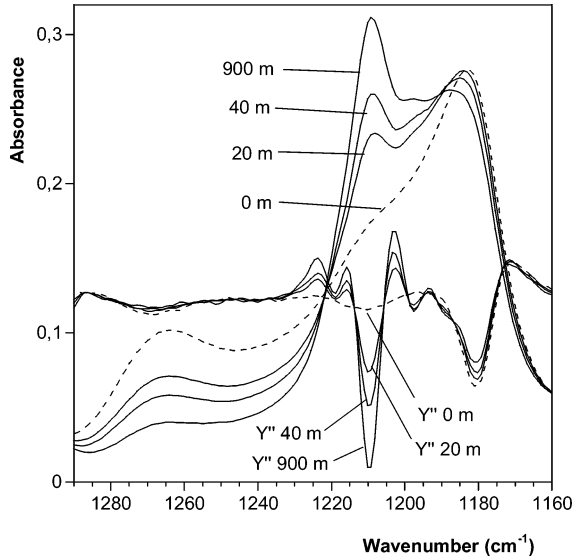

Figure 11. Ester C−O stretching region of PLLA and second derivatives recorded during isothermal crystallization at 200 °C. The spectrum of completely amorphous blend is highlighted with a dotted line.

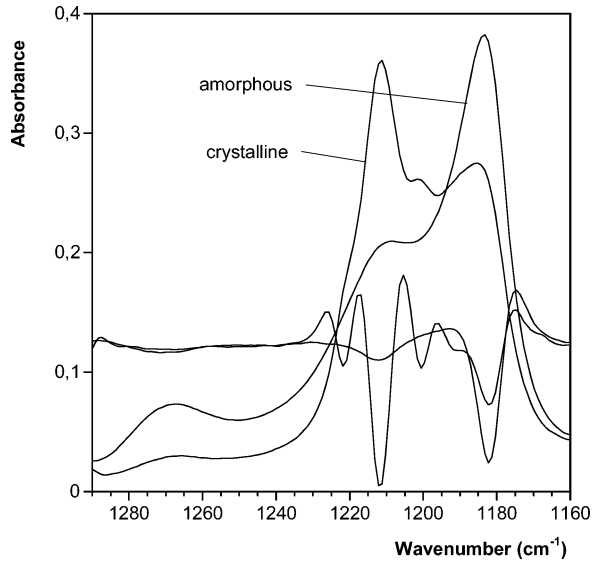

Figure 12. Ester C−O stretching region of PLLA and second derivatives recorded at room temperature before and after isothermal crystallization at 150 °C for 15 h.

higher temperatures show an enhanced intensity change from the band at 1182 to the band at 1212 cm^{-1} (see spectra c and d in Figure 8).

Similarly to the case of the stereocomplex, new bands appear at about 1198 and 1219 cm^{-1} during crystallization, which can be attributed to factor group splitting. At the crystallization temperature, the new bands show low intensities that are enhanced on cooling. Figure 12 shows the spectrum of PLLA crystallized at 150 °C recorded at room temperature. The spectrum shows the two pairs of factor group split bands located at 1222/1212 and 1200/1182 cm^{-1}. Compared to the spectrum of the stereocomplex, in crystalline PLLA the components located in the initial wavenumbers show higher relative intensities than the new bands appearing during crystallization. In addition, bands at the original locations are also somewhat broader than the new bands (the band at 1182 cm^{-1} shows also a shoulder at 1190 cm^{-1}). Hence, bands located at the original wavenumbers should be attributed to both the amorphous and

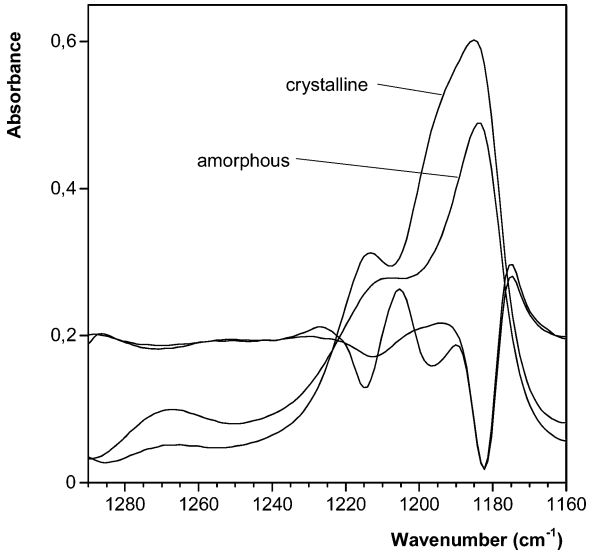

Figure 13. Ester C−O stretching region of PLLA and second derivatives recorded at room temperature before and after isothermal crystallization at 90 °C for 1 h.

crystalline phases. As discussed before, melt crystallization of PLLA leads to a semiordered interlamellar material that shows narrow bands after crystallization. The overlap of these narrow bands with the low wavenumber components of the factor group split pairs results in a enhanced intensity of these components. Regarding the shoulder at 1190 cm^{-1}, it is probably originated by the same vibrational mode responsible for the asymmetry observed in the parallel band of amorphous PLLA (this component is skewed to the higher wavenumber side; see Figure 12). Transition dipole coupling (TDC) interactions can shift to higher wavenumbers absorptions due to parallel components[11] (they have no effect on the location of perpendicular components). The strength of dipole−dipole interactions strongly depends in the relative orientation of interacting groups, being particularly strong for highly aligned systems.[49] The transition moment of the C−O stretching mode of chains in the all-trans conformation is known to be mainly parallel to the chain axis;[50,51] hence, the shoulder at 1190 cm^{-1} probably arises from tt conformers in the semiordered interlamellar material.

In summary, crystallization leads again to a semiordered interphase, resulting in narrower bands. These bands are strongly overlapped with the lower wavenumber components of the factor group split bands, resulting in enhanced intensities. Factor group splitting of 10 and 18 cm^{-1} are observed for the perpendicular and parallel bands, respectively, at room temperature (Figure 12). Finally, the parallel band shows additional splitting, probably due to shifting to higher wavenumers due to TDC interactions.

Figure 13 shows the spectra of PLLA cold crystallized at 90 °C for an hour. For brevity, we show only the spectra obtained at room temperature before and after crystallization. As can be seen factor group splitting is again obtained in the parallel component, but bands are broader and shift decreases to 12 cm^{-1} for this component. Both factors are indicative of lower crystalline perfection. In addition, factor group splitting is not observed for the perpendicular component, a result consistent with that observed in the C═O stretching region. The only perpendicular band that can be observed in the IR spectrum is located at an intermediate wavenumber (∼1215 cm^{-1}), representing the mean factor group split for the distribution of crystalline perfection present in the sample.

Conclusions

The analysis of the infrared spectrum of crystalline PLLA samples is consistent with the existence of two crystalline morphologies. The curved morphology of less perfect crystals in the core region of spherulites is responsible for their lower thermal stability relative to the crystals located in the outer regions. Hence, DSC traces show double melting peak attributed to both crystalline morphologies. The analysis of the IR spectrum of crystalline PLLA samples accounts for these morphologies. Factor group splitting is observed in both the C═O and ester C−O stretching regions. In both spectral regions, splitting of the perpendicular component is highly sensitive to crystalline order and therefore can be used to assess crystallinity perfection.

The C═O stretching region shows a complex profile that can be interpreted assuming intramolecular coupling, factor group splitting, and a semiordered interphase between the lamellar stacks formed at high crystallization temperatures. Splitting phenomena in the C═O stretching region should not be attributed to different crystals modifications. The same 10_3 helix conformation has been reported for both of them, and similar intermolecular interactions should be also expected. IR spectroscopy is highly sensitive to conformation and specific interactions but has a limited sensitivity to long-range order.

Acknowledgment. The authors are thankful for financial support from the Basque Government, Dpt. of Industry, Trade and Tourism (project IE03-105), The University of Basque Country (Project UPV 05/130), and MCYT (Project MAT2005-08347-C02-01).

Appendix. IR Intensity and Crystal Orientation

The intensity of an IR band is the square of the scalar product of the transition dipole moment vector **R** by the electric field vector **E**:

$$I = (\vec{\mathbf{E}}\cdot\vec{\mathbf{R}})^2 \tag{A1}$$

We will apply this expression to obtain the intensity changes accompanying the crystallization process, considering the orientation adopted by the lamellar crystals in each case. Let us recall that the transition moment corresponding to the C═O stretching mode of gt conformers is perpendicular to the helical chain.

Flat-On Crystals. Let us assume a fully crystalline PLLA sample, consisting only of flat-on crystals. The sample lies on the *XY* plane, and the incident beam goes in the *Z* direction. Excluding the folding points in the top and bottom surfaces of the lamellae, all the chains are oriented in the *Z* direction, and all the transition moments lie in the *XY* plane. In this case, the angle between the electric field and the absorbing transition moment will always be zero and

$$I = |\mathbf{E}|^2|\mathbf{R}|^2 \tag{A2}$$

Amorphous Sample. Again, let us assume a fully amorphous sample lying on the *XY* plane and the incident beam going in the *Z* direction (Figure 14a). A random distribution of transition moment can be assumed in the amorphous sample. All the transition moments with the same θ angle will give the same intensity (in other words, all show the same projection in the *XY* plane). The probability of a transition moment to be located in the fringe dθ (Figure 14) will be proportional to $[(2\pi \cos\theta\ \mathrm{d}\theta)/(4\pi)]$ (where the numerator is the area of the fringe and the denominator is total solid area or the total area of integration). The mean intensity considering the relative probability of each possible orientation is

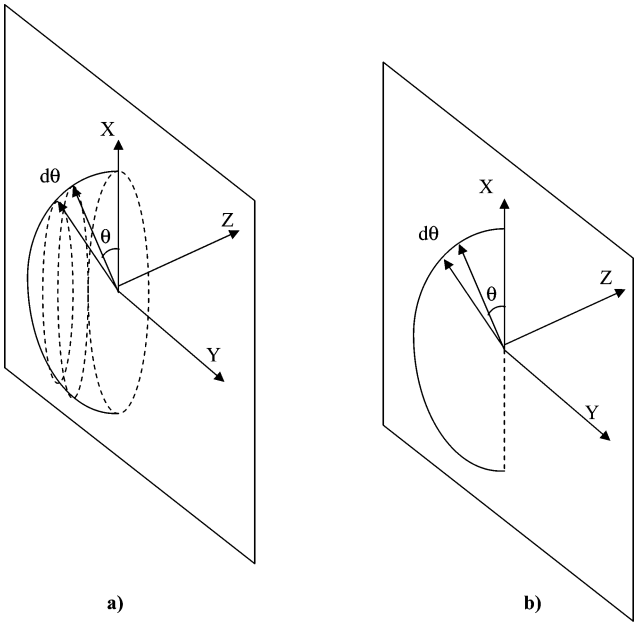

Figure 14. Spatial orientation of transition moments in (a) random 3D arrangement and (b) edge-on helical chains in the *Y*-axis direction.

$$I = \frac{2\pi}{4\pi}\int_{-\pi/2}^{\pi/2}|\mathbf{E}|^2|\mathbf{R}|^2\cos^3\theta\ \mathrm{d}\theta \tag{A3}$$

Integrating

$$I = \frac{1}{2}|\mathbf{E}|^2|\mathbf{R}|^2\left[\sin\theta - \frac{\sin^3\theta}{3}\right]_{-\pi/2}^{\pi/2} \tag{A4}$$

Hence

$$I = \frac{2}{3}|\mathbf{E}|^2|\mathbf{R}|^2 \tag{A5}$$

This result implies that when a fully amorphous sample crystallizes to a sample consisting only on flat-on crystals, its intensity increases from a relative value 2/3 to a relative value 1.0. The percent area increase is $[(1 - 2/3)/(2/3)] \times 100 = 50\%$

Edge-On Crystals. Again, it is assumed a 100% crystalline sample lying in the *XY* plane (Figure 14b). For simplicity, let us assume that all the chains go in the *Y* axis direction. The transition moments can be spread over 2π radians in the *ZX* plane (see Figure 14). The probability of a transition moment to be located into a (dθ) arc is proportional to (d$\theta/2\pi$). The mean intensity considering the relative probability of each possible orientation is

$$I = \frac{1}{2\pi}\int_0^{2\pi}|\mathbf{E}|^2|\mathbf{R}|^2\cos^2\theta\ \mathrm{d}\theta \tag{A6}$$

Integrating

$$I = \frac{1}{2\pi}|\mathbf{E}|^2|\mathbf{R}|^2\left[\frac{1}{2}\theta + \frac{1}{2}\sin\theta\cos\theta\right]_0^{2\pi} \tag{A7}$$

Hence

$$I = \frac{1}{2}|\mathbf{E}|^2|\mathbf{R}|^2 \tag{A8}$$

Thus, if a fully amorphous sample crystallizes to a sample consisting only of edge-on crystals, its intensity decreases from a relative value 2/3 to a relative value 1/2. The percent change of area is $[(1/2 - 2/3)/(2/3)] \times 100 = -25\%$ (area decreases 25%).

References and Notes

(1) Doi, Y. *Microbial Polyesters*; VCH Publishers: New York, 1990.
(2) Bergsma, J. E.; Bos, R. R. M.; Rozema, F. R.; Jong, W. D.; Boering, G. *J. Mater. Sci.: Mater. Med.* **1996**, *7*, 1.
(3) Fambri, L.; Pergoretti, A.; Fenner, R.; Incardona, S. D.; Migliarisi, C. *Polymer* **1997**, *38*, 79.
(4) Sinclair, R. G. *Pure Appl. Chem.* **1996**, *A33*, 585.
(5) Hoogsteen, W.; Postema, A. R.; Pennings, A. J.; Brinke, G. T.; Zugenmaier, P. *Macromolecules* **1990**, *23*, 634.
(6) Kister, G.; Cassanas, G.; Vert, M. *Polymer* **1998**, *39*, 267.
(7) Zhang, J.; Tsuji, H.; Noda, I.; Ozaki, Y. *J. Phys. Chem. B* **2004**, *108*, 11514.
(8) Zhang, J.; Tsuji, H.; Noda, I.; Ozaki, Y. *Macromolecules* **2004**, *37*, 6433.
(9) Zhang, J.; Duan, Y.; Sato, H.; Tsuji, H.; Noda, I.; Yan, S.; Ozaki, Y. *Macromolecules* **2005**, *38*, 8012.
(10) Aou, K.; Hsu, S. L. *Macromolecules* **2006**, *39*, 3337.
(11) Meaurio, E.; Zuza, E.; López-Rodríguez, N.; Sarasua, J. R. *J. Phys. Chem. B* **2006**, *110*, 5790.
(12) Davison, W. H. T. *J. Chem. Soc.* **1951**, 2456.
(13) Popov, E. M.; Khomenko, A. K.; Shorygin, P. P. *Ser. Khim.* **1965**, *1*, 51.
(14) Tam, C. N.; Bour, P. B.; Keiderling, T. A. *J. Am. Chem. Soc.* **1996**, *118*, 10285.
(15) Miyazawa, T. *J. Phys. Chem.* **1960**, *32*, 1647.
(16) Miyazawa, T.; Blout, E. R. *J. Am. Chem. Soc.* **1961**, *83*, 712.
(17) Brauner, J. W.; Flach, C. R.; Mendelsohn, R. *J. Am. Chem. Soc.* **2005**, *127*, 100.
(18) Brauner, J. W.; Dugan, C.; Mendelsohn, R. *J. Am. Chem. Soc.* **2000**, *122*, 677.
(19) Huang, R.; Kubelka, J.; Barber-Armstrong, W.; Silva, R. A. G. D.; Decatur, S. M.; Keiderling, T. A. *J. Am. Chem. Soc.* **2004**, *126*, 2346.
(20) Paul, C.; Wang, J.; Wimley, W. C.; Hochstrasser, R. M.; Axelsen, P. H. *J. Am. Chem. Soc.* **2004**, *126*, 5843.
(21) Sarasua, J. R.; López-Rodríguez, N.; López-Arraiza, A.; Meaurio, E. *Macromolecules* **2005**, *38*, 8362.
(22) Kim, Y. J.; Chang, H.-C.; Sullivan, V. S.; Jonas, J. *J. Chem. Phys.* **1999**, *111*, 9658.
(23) Theimer, O. *J. Chem. Phys.* **1957**, *27*, 408.
(24) Zbinden, R. *J. Mol. Spectrosc.* **1959**, *3*, 654.
(25) Snyder, R. G. *J. Mol. Spectrosc.* **1960**, *4*, 411.
(26) Snyder, R. G.; Schachtschneider, J. H. *Spectrochim. Acta* **1963**, *19*, 85.
(27) Schindler, A.; Harper, D. H. *J. Polym. Sci., Polym. Chem. Ed.* **1979**, *17*, 2593.
(28) Wang, Y.; Mano, J. F. *Eur. Polym. J.* **2005**, *41*, 2335.
(29) Savitzky, A.; Golay, M. J. E. *Anal. Chem.* **1964**, *36*, 1627−1639.
(30) Steiner, J.; Termonia, Y.; Deltour, J. *Anal. Chem.* **1972**, *44*, 1906−1909.
(31) Meaurio, E.; Zuza, E.; Sarasua, J. R. *Macromolecules* **2005**, *38*, 1207.
(32) Bernal-Lara, T. E.; Liu, R. Y. F.; Hiltner, A.; Baer, E. *Polymer* **2005**, *46*, 3043.
(33) Wang, Y.; Ge, S.; Rafailovich, M.; Sokolov, J.; Zou, Y.; Ade, H.; Lüning, J.; Lustiger, A.; Maron, G. *Macromolecules* **2004**, *37*, 3319.
(34) Kikkawa, Y.; Abe, H.; Fujita, M.; Iwata, T.; Inoue, Y.; Doi, Y. *Macromol. Chem. Phys.* **2003**, *204*, 1822.
(35) Ivanov, D. A.; Pop, T.; Yoon, D. Y.; Jonas, A. M. *Macromolecules* **2002**, *35*, 9813.
(36) Haubruge, H. G.; Daussin, R.; Jonas, A. M.; Legras, R. *Polymer* **2003**, *44*, 8053.
(37) Lee, B.; Shin, T. J.; Lee, S. W.; Yoon, J.; Kim, J.; Ree, M. *Macromolecules* **2004**, *37*, 4174.
(38) Lagaron, J. M.; Powell, A. K.; Davidson, N. S. *Macromolecules* **2000**, *33*, 1030.
(39) Lagaron, J. M. *Macromol. Symp.* **2002**, *184*, 19.
(40) Peter, D. *J. Phys. Chem. Sol.* **1975**, *36*, 1401.
(41) Snyder, R. G. *J. Chem. Phys.* **1967**, *47*, 1316.
(42) Hagemann, H.; Snyder, R. G.; Peacock, A. J.; Mandelkern, L. *Macromolecules* **1989**, *22*, 3600.
(43) Lauritzen, J. I.; Hoffman, D. J. *J. Appl. Phys.* **1973**, *44*, 4340.
(44) Iannace, S.; Nicolais, L. *J. Appl. Polym. Sci.* **1997**, *64*, 911.
(45) Snyder, R. G.; Maroncelli, M.; Strauss, H. L.; Hallmark, V. M. *J. Phys. Chem.* **1986**, *90*, 5623.
(46) Sarasua, J. R.; Prud'homme, R. E.; Wisniewski, M.; Le Borgne, A.; Spassky, N. *Macromolecules* **1998**, *31*, 3895.
(47) Yasuniwa, M.; Tsubakihara, S.; Youhei, S.; Chitoshi, N. *J. Polym. Sci., Part B* **2004**, *42*, 25.
(48) Silverstein, R. M.; Webster, F. X.; Kiemle, D. J. *Spectrometric Identification of Organic Compounds*, 7th ed.; John Wiley & Sons: New York, 2005.
(49) Painter, P. C.; Pehlert, G. J.; Hu, Y.; Coleman, M. M. *Macromolecules* **1999**, *32*, 2055.
(50) Bradbury, E. M.; Elliott, A.; Fraser, R. D. B. *Trans. Faraday Soc.* **1960**, *56*, 1117.
(51) Brauner, J. W.; Flach, C. R.; Xu, Z.; Bi, X.; Lewis, R. N. A. H.; McElhaney, R. N.; Gericke, A.; Mendelsohn, R. *J. Phys. Chem. B* **2003**, *107*, 7202.
(52) Cho, T. Y.; Strobl, G. *Polymer* **2006**, *47*, 1036.
(53) Mano, J. F.; Wang, Y.; Viana, J. C.; Denchev, Z.; Oliveira, M. J. *Macromol. Mater. Eng.* **2004**, *289*, 910.
(54) Fischer, E. W.; Stertzel, H. J.; Wegner, G. *Kolloid-Z. Z. Polym.* **1973**, *251*, 980.

MA061890R